

## Fatigue behaviour of non-welded wrapped composite joints for steel hollow sections in axial load experiments

Feng, Weikang; Pavlovic, Marko

**DOI**

[10.1016/j.engstruct.2021.113369](https://doi.org/10.1016/j.engstruct.2021.113369)

**Publication date**

2021

**Document Version**

Final published version

**Published in**

Engineering Structures

**Citation (APA)**

Feng, W., & Pavlovic, M. (2021). Fatigue behaviour of non-welded wrapped composite joints for steel hollow sections in axial load experiments. *Engineering Structures*, 249, 1-14. Article 113369. <https://doi.org/10.1016/j.engstruct.2021.113369>

**Important note**

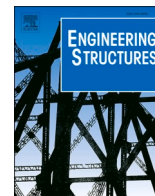
To cite this publication, please use the final published version (if applicable). Please check the document version above.

**Copyright**

Other than for strictly personal use, it is not permitted to download, forward or distribute the text or part of it, without the consent of the author(s) and/or copyright holder(s), unless the work is under an open content license such as Creative Commons.

**Takedown policy**

Please contact us and provide details if you believe this document breaches copyrights. We will remove access to the work immediately and investigate your claim.



# Fatigue behaviour of non-welded wrapped composite joints for steel hollow sections in axial load experiments

Weikang Feng, Marko Pavlovic\*

Faculty of Civil Engineering and Geoscience, Delft University of Technology, 2600AA Delft, the Netherlands

## ARTICLE INFO

### Keyword:

Wrapped composite joint  
Bonded joint  
CHS  
Steel-composite  
Fatigue experiments  
GFRP  
Crack growth  
3D DIC  
Welded joint  
Surface roughness

## ABSTRACT

Design and execution of fatigue load dominated circular hollow section (CHS) multi-membered structures, such as offshore jacket and floating structures for wind turbines, truss bridges, etc., is hinged on fatigue performance of critical welded joints. An innovative jointing technology of wrapped composite joint connects steel hollow sections by direct bonding through a fibre reinforced polymer composite wrap, which completely avoids welding and therefore has superior fatigue performance than welded joints. In this study first results on fatigue performance of the wrapped composite joints is presented. Tensile cyclic loading tests on wrapped composite X-joint specimens were carried out to characterise their fatigue performance under different constant amplitude load ranges and compare it to equivalent welded joints. In addition, the influence of surface roughness of steel tubes and re-testing (load history) on fatigue performance of wrapped composite joints, as well as the influence of fatigue loading on residual static resistance was investigated in experiments. Preliminary S-N curves of wrapped composite joints are established. The tests results showed that X45 wrapped composite joints exhibited steadier stiffness degradation and 10–100 times longer fatigue life than their welded equivalents. Through 3D DIC surface strain measurements and post-failure microscopic insights to cut specimens, different failure modes including debonding at glass fibre composite-to-steel interface, delamination/fracture of the composite layers and fracture of steel brace are distinguished. The relationship between joint stiffness degradation rates, crack propagation rates and nominal stress ranges in the brace are established, based on which a preliminary fatigue life prediction of wrapped composite joints can be made. The re-tested specimens exhibited superior fatigue performance than virgin ones, while specimens with poor steel surface roughness showed worse fatigue performance. After fatigue loading with 40% of stiffness degradation, the specimens were found to still have the potential to sustain its original static resistance.

## 1. Introduction

Due to favourable mechanical efficiency about multiple axes, circular hollow sections (CHS) are widely used for steel truss/jacket supporting structures of off-shore wind turbines, oil and gas platforms, steel bridges, etc. The field of floating structures supporting wind turbines and other renewable energy converters offshore is placing even higher demands on fatigue performance of the multi-membered structures. Current limitation to improve the durability and cost effectiveness of multi-membered CHS structures is the low fatigue endurance of their welded joints due to the reduced fracture toughness and stress concentration resulting from local bending of thin walled truss members in the joint region [1]. Thick profiles need to be used in combination with costly welding procedures to satisfy fatigue endurance driven design of

such structures. An existing alternative are the casted joints [2] lagging in large scale application in offshore market. In this paper, an innovative concept was introduced where bonding is used to connect the CHS members through FRP composite wrap, without welding, to create fatigue resistant CHS joints.

In recent years, the use of fibre reinforced polymer (FRP) composite materials has gained worldwide attention in the field of structural engineering [3]. Different from conventional metal materials, the corrosion resistance, high fatigue endurance, light weight, high strength-to-weight ratio and tailorability, favor use of FRPs in various demanding engineering applications, such as wind turbine blades. One use of specific properties of composites is to strengthen tubular steel structures. The excellent shape formability during production makes it efficient and convenient way to strengthen the welded tubular joints, which generally

\* Corresponding author.

E-mail address: [M.Pavlovic@tudelft.nl](mailto:M.Pavlovic@tudelft.nl) (M. Pavlovic).

<https://doi.org/10.1016/j.engstruct.2021.113369>

Received 15 April 2021; Received in revised form 22 September 2021; Accepted 12 October 2021

Available online 22 October 2021

0141-0296/© 2021 The Authors. Published by Elsevier Ltd. This is an open access article under the CC BY license (<http://creativecommons.org/licenses/by/4.0/>).

have complex geometry. By now, experimental and numerical investigations have been conducted on externally strengthened welded tubular joints with different kinds of geometries, such as butt-welded [4,5], T-shaped [6,7], Y-shaped [8] or K-shaped [9,10]. Their axial/bending bearing capacity has been proved to be enhanced and their overall joint behaviour to be improved by such composite-bonding measures. While exhibiting enhanced mechanical performance, existing composite-strengthened tubular joints still use welding for main load transferring mechanism, which remains to be the source of stress concentration and brittle fatigue failure. An innovative solution has been proposed at TU Delft [11] in form of non-welded wrapped composite joints that utilize bonding between composites and steel to transfer the joint loads. Composite wrap is employed to connect the hollow section brace members to the chords directly in complex CHS joints (Fig. 1). Monotonic tensile tests on joints have been conducted and results have also proved their improved stiffness, equivalent static resistance and superior fatigue performance compared to welded joints [12,13].

While showing very good static behaviour, the newly proposed wrapped composite joints have not been understood yet in terms of their fatigue behaviour. It is of vital importance to clarify their law of stiffness degradation, failure modes and corresponding deterioration process when subjected to cyclic loading. Considering that two typical failure modes were shown in static tests: fracture of the composite wrap and debonding at the composite-to-metal interface [12,13], attention needs to be paid on these two mechanisms under fatigue loadings as well. As for fatigue performance of the composite material, which is relevant for failure mode of the composite wrap, the existing literature mainly focuses on plated (flat) specimens. The composite wrap in the wrapped composite joints has complex geometry of variable thickness and double curvature and with complex ply-drops and stacking sequence influencing multiple and variable fibre directions across the surface and through the thickness. However, several of those factors have been studied separately by previous researches. For example the thickness of the lamination [14,15], a slightly increase of which can lead to significant improvement of flexural behaviour of bi-woven glass fibre laminated composites. Fibre arrangement also influences a lot, specimens with  $[0/90^\circ]$  orientation exhibited much longer fatigue life under the

same load range than specimens with  $[45/-45^\circ]$  plies [16,17]. Volume fraction is another factor. As volume fraction increases, the stiffness degradation rate due to fatigue loading decreases, although research [18,19] indicate there is a cap at about 40% fibre volume fraction, above which the stiffness degradation rate may increase again due to decrease of bonding strength of the composite materials. In addition to these factors, attention needs to be paid on the detrimental effects of stress concentration resulting from defects like wrinkles, fibre misalignments, and voids introduced during the fabrication process. These defects may favour earlier develop to failure mechanisms like matrix cracking, fibre breakage, debonding, transverse-ply cracking, interface cracking, etc., which then will be sources of micro-buckling, translaminar crack growth and delamination [20–22]. Although fatigue behaviour of composite materials has been studied extensively as shown above, further investigation still needs to be conducted in terms of fatigue performance of wrapped composites with complicated geometry loaded under combined forces. Besides fatigue behaviour of composite materials, fatigue behaviour of composite-to-metal bonded joints has also attracted attention from researchers. Some researchers [23,24] found that at low-level of fatigue loads (the maximum cyclic load range less than 40–50% of the static strength), the influence of fatigue load on strength or stiffness of the joint is insignificant. But generally, the stiffness of the joints will decrease as the number of fatigue load cycle increases as the consequence of debonding on the interface. Normally the degradation process can be divided into 3 stages: the initiation stage with a stiffness degradation of about 10%, propagation stage with steady stiffness degradation, and a final stage leading to complete debonding and failure [25,26]. It was also found that the stiffness degradation rate increases with the increment of stress level and meanwhile, quantitative relationship between stiffness degradation rate and stress level has also been proposed by the authors. Other researchers also focused on another important factor that may influence fatigue behaviour of the bonded composite-to-steel joints, i.e. roughness of the steel surfaces. Under mixed mode fatigue load, it was found that the threshold value of strain energy release rate  $G_{th}$  increases with the roughness but will reach a plateau at  $R_a = 3.9\text{--}6.4\ \mu\text{m}$  [27]. But the influence of surface roughness on crack growth rate decreased at relatively high crack growth rate due to

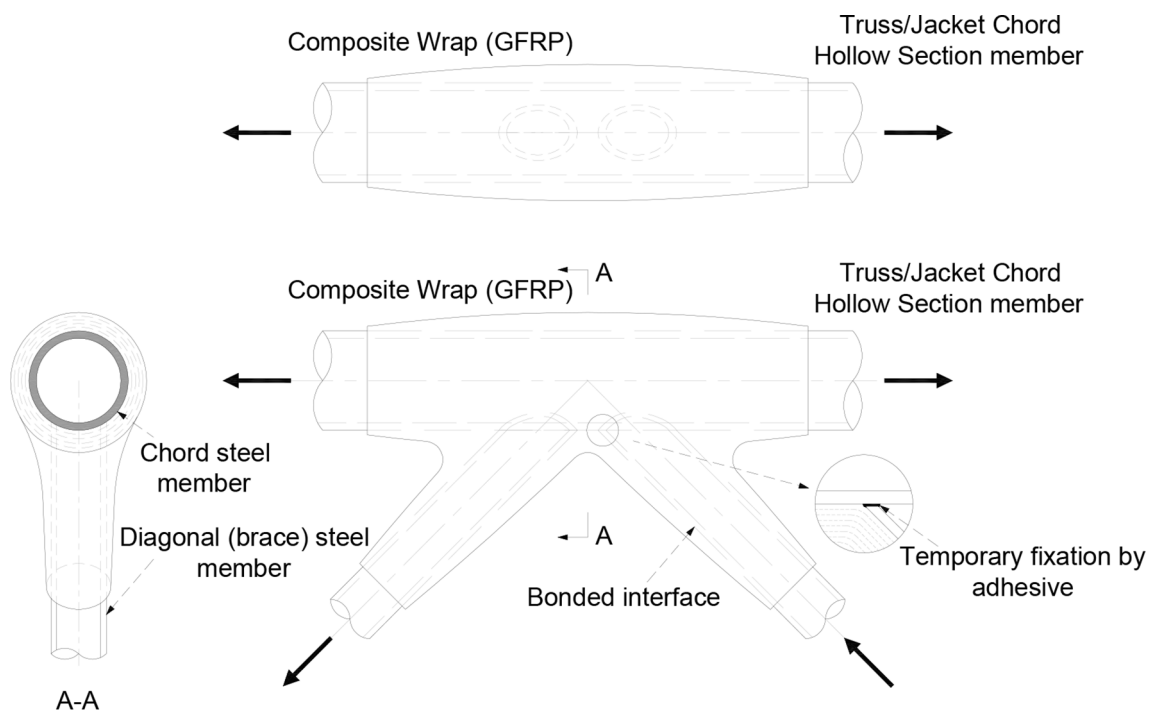


Fig. 1. Layout of the wrapped composite joint – example of K-joint geometry.

the crack path shifting farther from the interface as the strain energy release increased. It should be noted that different substrate materials with different surface treatments were found to have different optimum  $R_a$  values in terms of their static or fatigue performance and some even don't have it [28–30]. As stated above, the surface treatment also has significant influence on the fatigue behaviour. For example, some researchers found that grit blasting together with sand blasting showed better fatigue performance than bristle blasting [31]. Number of researchers have carried out numerical modelling of the debonding process to better understand the stress distribution at the interface. The most common technique for simulating debonding is the Cohesive Zone Model (CZM), which is described by traction-separation law and can be used to reflect progressive damage of the interface [32]. Another commonly used method called Visual Crack Closure Technique (VCCT) [32] allows implementation of Paris law and degradation modelling by fracture mechanics and cycle jumping.

The debonding failure at the interface is brittle failure mode and hard to be detected, therefore more detrimental than the fracture of the composite material. From the conceptual design viewpoint, the debonding failure should be avoided in wrapped composite joints while material failure should be dominant. In addition, the circumferential welds are inevitable in the full-scale offshore structures to form the CHS tubes of 1–2 m diameter and assemble the members to prefabricated wrapped composite joints. The aim is to design and produce wrapped composite joints at the full scale which have longer fatigue life than the circumferential welds. In the first phase of the research, it is chosen to focus on investigating the unfavourable debonding failure mode, while fracture of the FRP composite material is avoided by using relatively large thickness of the wrapping.

In this paper fatigue tests have been conducted for wrapped composite joints and their welded equivalents. Their stiffness degradation and failure modes were extensively compared. During fatigue tests, strain distribution of wrapped composite joints were recorded by 3D DIC system and used to analyse crack propagation. The relationship is established between stiffness degradation rate and crack propagation rate, vs. nominal stress range in the brace. The influence of re-testing (load history) on fatigue performance of wrapped composite joints and the influence of fatigue loading on their residual static resistance were investigated. Furthermore, preliminary S-N curves were established for wrapped composite joints. Then the joints were cut into several pieces through their mid-plane so that the failure modes at microscale and morphology of the composite-to-steel interface were inspected further. Combined with the roughness measurement, the influence of morphology of the steel surfaces on their fatigue behaviour has been discussed.

## 2. Test specimens

Two types of specimens, wrapped composite joints and welded joints, are used in this study, as shown in Table 1 and Fig. 2. These specimens are produced by joining two circular hollow section (CHS) brace members  $\text{Ø}60.3 \times 4$  to the chord made of CHS profile  $\text{Ø}108 \times 5$  with the intersection angle of  $45^\circ$  by welding (for welded joints) and glass fibre composite wrapping (for wrapped composite joints), respectively. Such X-joint geometry with larger diameter of the middle CHS and  $45^\circ$  angle, is chosen to represent K-joints in terms of stress concentrations. For welded joints, the chord and braces were joined together by single sided, full penetration butt weld with the thickness of 4 mm, after which grinding of the weld toes was performed to improve its fatigue performance. For wrapped composite joints, surfaces of steel tubes of wrapped composite joints were grit blasted before wrapping and chemically degreased with acetone to ensure enough bonding strength between composite laminates and steel tubes. There is no separate adhesive layer between the composite wrap and the steel tubes. The composite wrap is directly laminated on the steel members. Therefore, the failure modes associated to the adhesive material are eliminated. The laminate of the composite wrap is

**Table 1**  
Load ranges and specimens.

Load range $\Delta F$ (kN)	Nominal stress range $\Delta\sigma_{nb}^1$ (MPa)	Specimens		Notes
		Welded joints	Wrapped composite joints	
6–66	85	wX45-Ss- T_F1	cX45-Ss- T_F1.1/2/3	Lower roughness
10–110	141	wX45-Ss- T_F2.1/2/3	cX45-Ss- T_F2.1a/2a cX45-Ss- T_F5.1/2/3	Higher roughness Lower roughness
15–165	212	—	cX45-Ss- T_F2.1b/2b cX45-Ss- T_F3.1/2/3 cX45-Ss- T_F4.1/2/3	Influence of re-testing Higher roughness Lower roughness

Naming rule: w - welded; c - wrapped composite; Ss - small scale; T - tensile test; F - fatigue test; SF - static test after fatigue loading

1. Nominal stress range in the brace, i.e.  $\sigma_{nb} = F/A$ , where  $A$  = cross section area of the brace.

formed with multi-directional composition of E-glass reinforcement and vinyl ester based thermoset resin system with fibre volume fraction ranging 30–32%. The wrapping thickness is maximum next to the root of the CHS braces with the nominal value of 14 mm and reduces to 0 mm at the composite wrap ends, see Fig. 2. The thickness in the narrow zone of the corner between brace and chord walls is even larger, up to 25 mm, due to the overlapping of the brace and chord composite layers. Such dedicated non-uniform thickness distribution of the composite wrap is used to optimize the load transfer mechanism by: 1. reducing stress concentrations in the composite wrap; 2. reducing concentrations of shear stresses at the bonded interface between the composite wrap and steel at the root of CHS braces and 3. eliminating peel stresses at the end of the composite wrap on the CHS braces. The production of specimens is made according to TU Delft procedure including hand-lamination and wrapping in specified subsequent lamination stages in controlled factory conditions at room temperature, with controlled route of surface preparation, roughness registration and quality control. The hand lamination procedure is done in several stages to ensure smooth thickness transition and ply drops, as well as good compaction and avoiding air gaps. Orientation of the of the fibres is chosen to result in predominantly quasi-isotropic GFRP laminate. No post-curing is applied to the joint specimens. It should be noted that all specimens are produced according to the same requirements. Two different batches are considered with focus on the influence of possible production quality deficiencies, namely different surface roughness of steel tubes, on fatigue performance of the wrapped composite joints. The average value of  $R_z$  in the batches with higher and lower surface roughness are  $R_z = 90 \mu\text{m}$  and  $R_z = 45 \mu\text{m}$ , respectively. More details about roughness measurements are given in Section 4.6. The steel profiles for specimens are mild steel grade S355. The material properties of composite laminates were obtained by standard tensile/compressive coupon tests according to ISO [33–35] and are summarised in Table 2. Specimens before wrapping and after being wrapped are shown in Fig. 3.

## 3. Test set-up, loading protocol and instrumentation

The tensile fatigue tests were conducted by the PCX 001 Hydraulic Wedge Grip in Stevin Lab II of Delft University of Technology. Its maximum loading capacity is 800kN for static test and  $\pm 600$  kN for dynamic test. During the tests, the ends of braces were clamped by tailor designed clamps fixed by the hydraulic jaws of the machine to introduce load to the specimens without involvement of any potentially limiting welded details, as shown in Fig. 4. The tests were carried out through force control at load frequency of 4 Hz, No significant heat-up effects

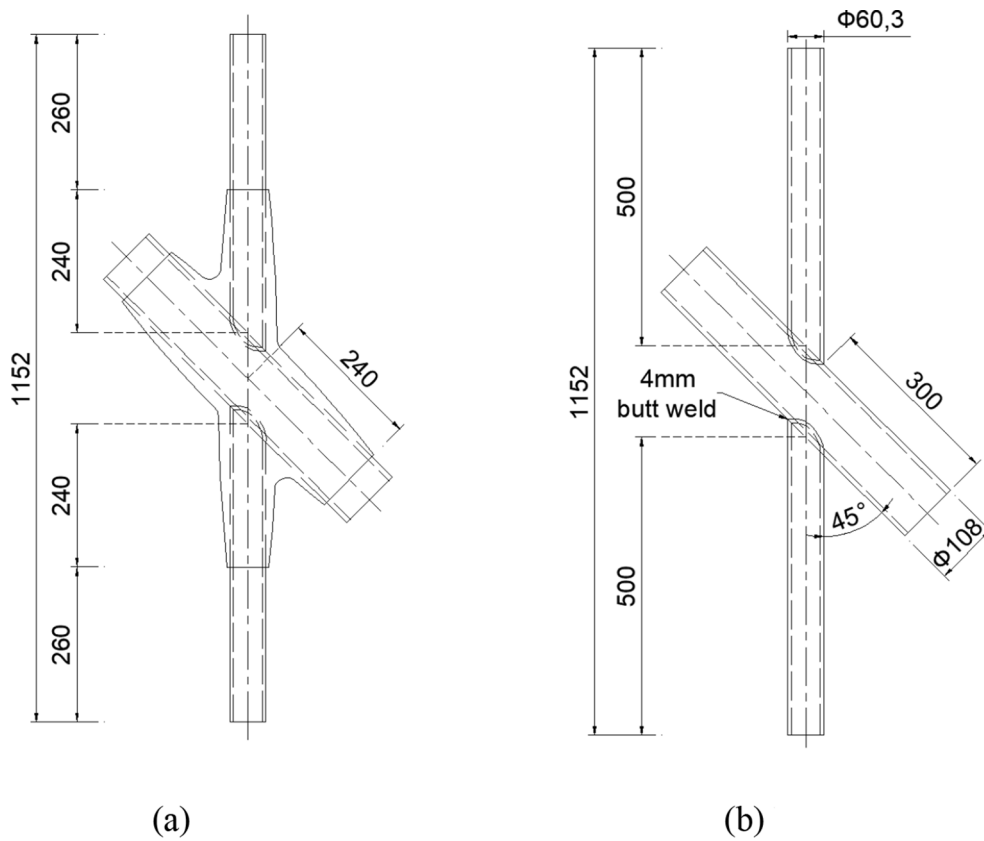


Fig. 2. Dimensions of specimens for axial fatigue tests. (a) wrapped composite joint (b) welded joint.

**Table 2**  
Material properties of the composite wrap laminate.

Mechanical property	Average value and (CoV)
Longitudinal and transverse compressive strength – $f_{x,c} = f_{y,c}$	200.11 MPa (3.79%)
Longitudinal and transverse compressive modulus – $E_{x,c} = E_{y,c}$	12077.11 MPa (4.50%)
Longitudinal and transverse tensile strength – $f_{x,t} = f_{y,t}$	216.18 MPa (5.78%)
Longitudinal and transverse tensile modulus – $E_{x,t} = E_{y,t}$	11798.20 MPa (6.37%)
Poisson's ratio – $\nu_{xy}$	0.15 (6.50%)
In-plane shear strength – $\tau_{xy}$	72.19 MPa (2.59%)
In-plane shear modulus – $G_{xy}$	3.12 MPa (6.81%)

(<5 °C) were noticed in the composite material at this testing frequency. Three different load ranges at load ratio of  $R = 0.1$  were considered for wrapped composite and welded joints as shown in Table 1. The tensile-tensile cyclic load on braces was considered as assumed to be most

adverse for debonding failure mode. The two lower load ranges, 6–66 kN and 10–110 kN, correspond to 88 MPa and 141 MPa nominal stress ranges in braces, respectively. Such regime was selected to reach the failure in welded joints at least 100,000 cycles considering stress concentration factor and S-N curves from DNV-RP-C203 (2016) [36]. At those two ranges, the wrapped composite joint reached no failure or significant crack development up to approx. 2–3 million cycles. Therefore, one step higher load range 15–165 kN, corresponding to nominal stress range in the steel brace member of 212 MPa, was used to develop wrapped composite joint degradation and study the failure behaviour. As shown in Table 1 and Table 2, for each load range 3 specimens of wrapped composite joints were tested. Welded joints are tested with total 4 specimens. The specimens, cX45-Ss-T\_F2.1/2 were tested under lower nominal stress range of 141 MPa in the first loading phase (named with ‘a’) and in the second phase under increased nominal stress range of 212 MPa (named with ‘b’) to accelerate the tests considering their negligible stiffness degradation in the first loading phase. The influence of re-testing was investigated meanwhile. All the specimens of wrapped

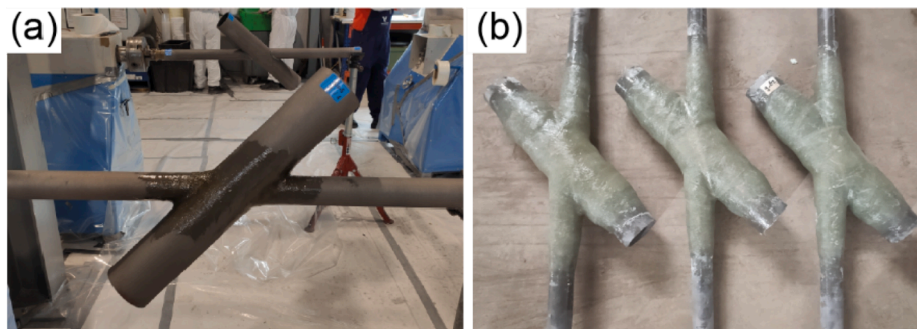


Fig. 3. Wrapped composite joints (a) before wrapping (b) after being wrapped.

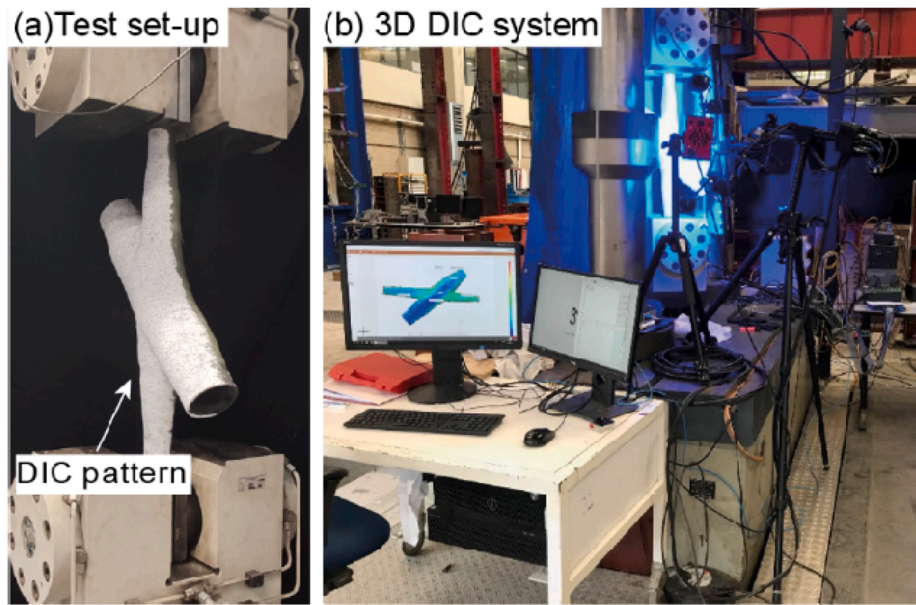


Fig. 4. Test set-up and 3D DIC system for fatigue tests.

composite joints are loaded up to 40% degradation of their initial stiffness measured between the loading points (end of the composite wrap). Afterwards monotonic static tensile load was applied until full joint failure to investigate the influence of cyclic loads on residual static behaviour by comparing to monotonic static load experiments with no prior cyclic loading. Few specimens failed by steel CHS outside composite wrap during cyclic loading and were not included in the follow-up static tests. The monotonic static load tests were displacement control with loading rate of 0.01 mm/s.

The displacement of the specimens and major strain of surfaces were measured by 3D Digital Image Correlation (DIC) system: GOM Aramis 12MP, adjustable base, 12 mm lenses + polarized blue led lights. DIC was used to monitor absolute and relative displacements along the specimen, strain concentrations, and crack propagation such that failure modes of the specimens can be observed real-time during the test, but also processed afterwards in more details. The spackle pattern is applied on one side of the specimen for the DIC system while the other side is left unpainted for visual observation of cracks in composite wrap. Stroke displacement and applied force measured by sensors inside the hydraulic actuator were used to control the test cyclic load application. The 3D DIC measuring system was coupled with the load-control system to drive the image acquisition throughout cycles by a threshold increment of the joint stiffness degradation, as shown in Fig. 4.

#### 4. Results and discussions

Welded joints failed at 350,000 and 70,000 cycles at two lower load ranges corresponding to 85 MPa and 141 MPa nominal stress ranges in braces, respectively. Crack initiation on the chord dominated the fatigue life followed by sudden propagation around circumference of the weld root and final failure. Wrapped composite joints at the same two lower load ranges did not fail up until 2–3 million cycles. Results are further studied in terms of stiffness degradation analysis and comparisons, failure mode characterization, influence of retesting and reduced surface roughness on stiffness degradation and definition of preliminary S-N curve for wrapped composite joints.

##### 4.1. Stiffness degradation

Stiffness of the joint  $k(n)$ , at a certain number of cycle  $n$ , can be calculated by:

$$k(n) = \frac{F_{\max}(n) - F_{\min}(n)}{\Delta L_{\max}(n) - \Delta L_{\min}(n)} \quad (1)$$

where  $F_{\max}(n)$  and  $F_{\min}(n)$  are the maximum and minimum applied forces at the  $n$ th cycle,  $\Delta L_{\max}(n)$  and  $\Delta L_{\min}(n)$  are the differences of displacements of the joint ends (elongations), at maximum and minimum load respectively. The  $k(n)$  in case of wrapped composite joint reflects the overall stiffness including both the wrapped part and steel tubes outside of the wrapped part. The same reference length, between the specimen ends, was used to present the stiffness degradation of welded joints for the comparison. During the loading process, stiffness of the wrapped composite joints degraded continuously due to crack initiation and propagation, i.e. debonding, at the composite-to-steel interface. Relative stiffness degradation of the specimens  $[k(n)/k(1)]$  under different nominal stress ranges is summarised in Fig. 5. Welded joints degenerated at a relatively slow rate during the crack initiation phase corresponding to approx. 80% of the total life. The second stage shows progressive stiffness degradation rate and sudden failure after 350,000 and 70,000 cycles, respectively. Under the same stress range, stiffness degradation of wrapped composite joints is much steadier. For specimens cX45-Ss-T\_F1.1/2/3, which were tested at nominal stress range of 85 MPa, there was only up to 2% stiffness degradation after 2 million cycles. The assumption is that they would have almost infinite fatigue life in laboratory conditions and further testing at this load range would be unfeasible. The tests at 85MP stress range were stopped after 2 million cycles. Specimens cX45-Ss-T\_F2.1/2 were initially loaded by applying the nominal stress range in the brace member of 141 MPa (results designated by ‘-a’). Again, a very limited (5–10%) degradation of stiffness was recorded after 3 mil cycles as shown in Fig. 5 (b) and no signs of cracks or delamination on the surface of the composite wrap. Therefore, the stress range was increased to 212 MPa (results designated by ‘-b’) to accelerate the test and investigate influence of re-testing on the fatigue performance. It took approximately additional 0.4 and 1.0 mil cycles until additional stiffness degradation of 20%, see Fig. 7. The influence of re-testing will be discussed in next section. Within specimens produced from the batch with lower surface roughness, namely cX45-Ss-T\_F5.1/2/3, stiffness degradation of 40% was achieved already after 200,000 to 400,000 cycles under the load range resulting in 141 MPa nominal stress range in the brace member. Under the nominal stress range of 212 MPa, the stiffness degradation of wrapped composite joints becomes more obvious. 40% stiffness degradation was reached at about

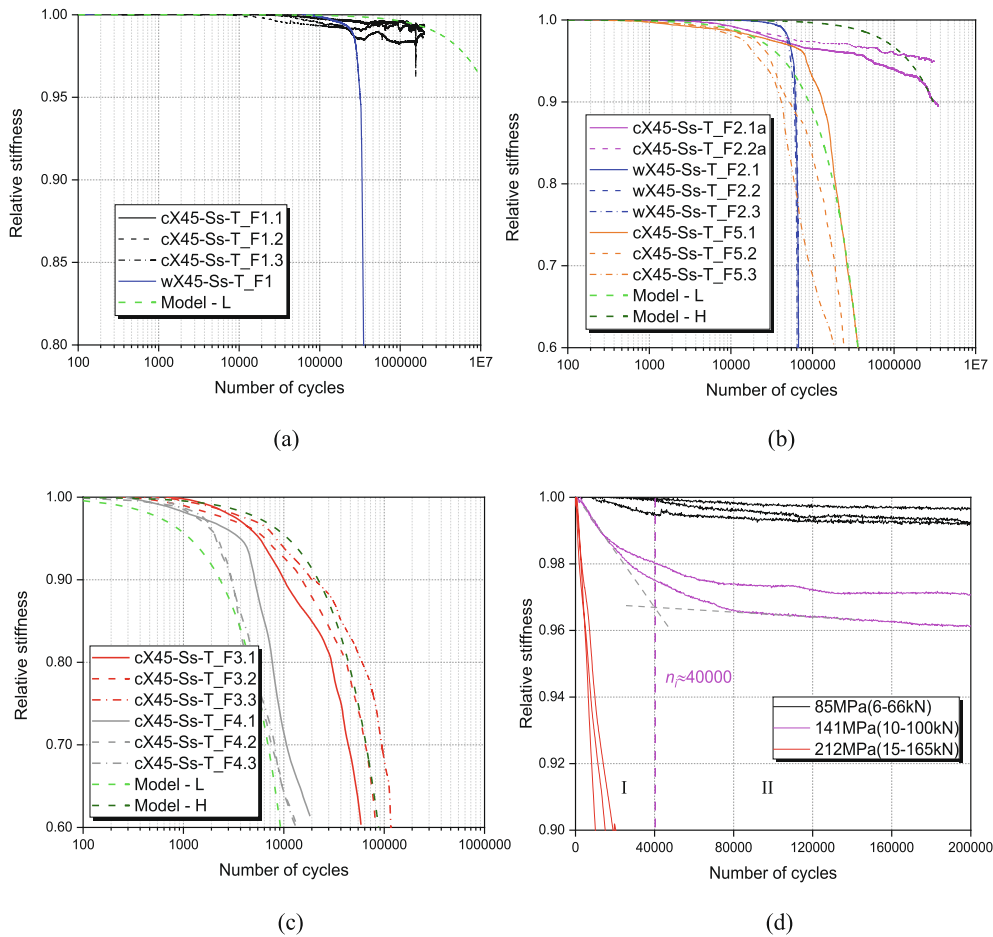


Fig. 5. Stiffness degradation of wrapped composite joints under different load ranges. (a) 6-66 kN ( $\Delta\sigma_{nb} = 85$  MPa) (b) 10-110 kN ( $\Delta\sigma_{nb} = 141$  MPa) (c) 15-165 kN ( $\Delta\sigma_{nb} = 212$  MPa) (d) initial degradation stage of wrapped joints.

60,000 to 100,000 cycles for the specimens cX45-Ss-T\_F3.1/2/3 with higher surface roughness. The specimens cX45-Ss-T\_F4.1/2/3, with lower surface roughness, reached 40% stiffness degradation at less than 20,000 cycles. Influence of roughness of the steel tubes is further discussed in Section 4.6. Stiffness degradation process of all the wrapped composite joints mentioned above is plotted in Fig. 5 (d) in linear scale where difference in stiffness degradation rates at different load/stress ranges are more noticeable. It can be shown that for specimens under nominal stress ranges of 85 MPa and 141 MPa the stiffness dropped by about 0.5% to 3% in the initial stage, respectively, after which a steady stiffness degradation stage followed. The initial stage is thought to be related to crack initiation at the composite-to-steel interface and the steady stage due to crack propagation [25]. By defining tangent lines of stiffness degradation curves at the initial and the following steady stage, the initiation life of these specimens can be obtained at the intersection point as shown in Fig. 5 (d). The initiation life of specimens under load ranges of 6-66kN and 10-110kN is around  $n_i = 40,000$ , which is negligible compared to their whole fatigue life dominated by steady propagation of the crack at the bonded interface. It should be noted that the initiation stage is not obvious for specimens under higher nominal stress range of 212 MPa.

Stiffness degradation rates of wrapped composite joints at the steady propagation stage were calculated and summarized in Table 3 for different nominal stress ranges in braces. As it would be expected, the stiffness degradation rate increases with the stress range. Considering that stiffness degradation is linear at the propagation stage, a linear model [25] was employed to quantitatively characterise stiffness degradation law of the wrapped composite joints. The model can be expressed as:

$$\frac{k(n)}{k(1)} = 1 - m_1 (\Delta\sigma_{nb})^{m_2} n \quad (2)$$

where parameters  $m_1$  and  $m_2$  can be obtained by curve fitting of experimental results and are assumed to be independent of number of cycles and nominal stress range. Based on Eq. (2), the fatigue life of the joint at a certain degree of stiffness degradation under a certain stress range can be calculated by:

$$n = \frac{k(1) - k(n)}{k(1)m_1 (\Delta\sigma_{nb})^{m_2}} \quad (3)$$

such that the S-N curve can be obtained for a certain stiffness degradation percentage. Relative stiffness degradation rates of specimens for the examined load ratio  $R = 0.1$  are plotted against nominal stress ranges in braces  $\Delta\sigma_{nb}$  in Fig. 6. Curve fitting was applied for specimens with 3 different nominal stress ranges with lower roughness and without re-testing (series F1.X, F4.X, and F5.X, see Table 1), and specimens with 2 different nominal stress ranges with higher roughness and without re-testing (F2.Xa and F3.X), respectively. Parameters  $m_1$  and  $m_2$  were determined as  $7.24e-29$  and  $10.22$  for specimens with lower roughness,  $4.68e-39$  and  $14.18$  for specimens with higher roughness, respectively. The influence of roughness will be further discussed in Section 4.6. Based on the parameters obtained above, stiffness degradation curves for specimens with higher (Model - H) and lower roughness (Model - L) according to the linear model depicted by Eq. (2) are shown in Fig. 5, which shows good match with test results.

**Table 3**  
Failure modes and stiffness degradation rates of wrapped composite specimens.

Load ranges $\Delta F$ (kN)	Nominal stress ranges $\Delta\sigma_{nb}$ (MPa)	Specimen	Failure modes	Stiffness degradation rate <sup>1</sup> (/cycle)	Average value (/cycle)	Note	
6–66	85	cX45-Ss-T_F1.1	De-bonding	2.51e-9	2.65e-9	Lower roughness	
		cX45-Ss-T_F1.2	De-bonding	3.14e-9			
		cX45-Ss-T_F1.3	De-bonding	2.30e-9			
10–110	141	cX45-Ss-T_F2.1a	De-bonding	1.97e-8	1.36e-8	Higher roughness	
		cX45-Ss-T_F2.2a	De-bonding	7.40e-9			
		cX45-Ss-T_F5.1	De-bonding	1.24e-6			
		cX45-Ss-T_F5.2	De-bonding	1.59e-6			
		cX45-Ss-T_F5.3	De-bonding	1.56e-6			
15–165	212	cX45-Ss-T_F2.1b	Fracture of steel tube*	4.77e-7	3.02e-7	Re-tested after F2.1a and F2.2a	
		cX45-Ss-T_F2.2b	De-bonding	1.27e-7			
		cX45-Ss-T_F3.1	De-bonding	6.29e-6		4.41e-6	Higher roughness
		cX45-Ss-T_F3.2	De-bonding	4.25e-6			
		cX45-Ss-T_F3.3	De-bonding*	2.69e-6			
		cX45-Ss-T_F4.1	De-bonding	2.48e-5			
		cX45-Ss-T_F4.2	De-bonding	2.59e-5			
		cX45-Ss-T_F4.3	De-bonding	3.25e-5			

1:  $[k(n_i)-k(n)]/[(n-n_i)k(1)]$

\* Specimens fully failed during fatigue loading.

4.2. Influence of re-testing

Load range for specimens cX45-Ss-T\_F2.1/2 was increased after no significant damage was observed after approx. 3 million cycles in order to demonstrate the impact of load history on fatigue performance of wrapped composite joints. Results are shown in Fig. 7. The re-tested specimens cX45-Ss-T\_F2.1b/2b performed better under the increased nominal stress range of 212 MPa than virgin specimens cX45-Ss-T\_F3.1/2/3 without previous load cycles. The same conclusion can be obtained from Table 3, where the average stiffness degradation rate of the re-tested specimens cX45-Ss-T\_F2.1b/2b is 3.02e-7/cycle, which is an order of magnitude lower than that of the virgin specimens, 4.41e-6/

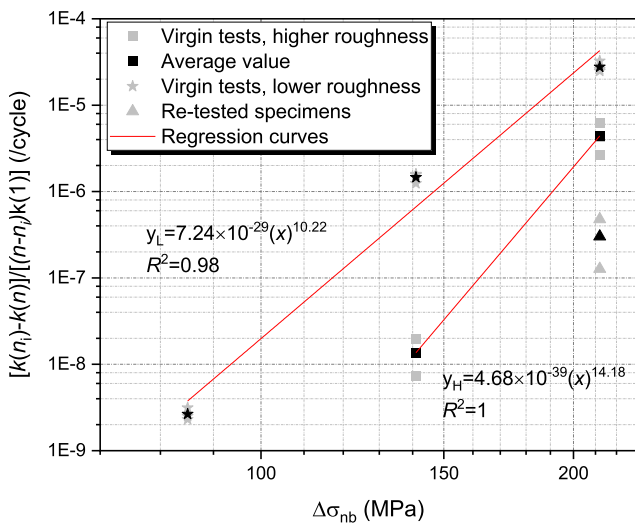


Fig. 6. Relationship between relative stiffness degradation rate and nominal stress range in function of surface roughness.

cycle. The hypothesis can be that initial low load range result in plasticization and favourable reduction of stress singularities at the bonded interface inside the root of the joint.

4.3. Failure modes and crack propagation analysis

The stiffness degradation of all virgin tested wrapped composite joint specimens was due to debonding of the interface between composite wrapping and steel profiles which is induced by the stress concentrations

at the composite-to-steel interface. Fig. 8 (a) shows a typical DIC contour plot of major principal strains corresponding to max load at a late stage of cyclic load. The zone of increased major principal strains on the surface of composite wrapping (light blue and green areas) is indicating the debonding inside the joint at the composite-to-steel interface. The debonding initiates at the root of braces CHS and propagates steadily towards the end of the composite wrapping on the brace member. The DIC contour plot in Fig. 8 (a) also indicates stress concentration in the sharp (acute) corner of the joint root between the brace and the chord wrapping. However, no significant surface cracks were observed in this region during cyclic loading.

Most of the wrapped composite joints didn't fully debond during the cyclic loading i.e. braces were not pulled out from composite wrapping. The cyclic loading was intentionally stopped at stiffness degradation up to 40% to perform monotonic test until failure and check residual static resistance. In average 80–100% of residual static resistance was obtained as shown in more details in Section 4.7. The exception is specimen cX45-Ss-T\_F3.3, which was left to fully debond during the cyclic tests and finally failed at 50% of stiffness degradation, as shown in Fig. 8 (b). One of the wrapped composite joint specimens, cX45-Ss-T\_F2.1b, failed suddenly at approx. 3 mil. load cycles at stiffness degradation of 30% due to fracture of the steel member at its end outside the wrapped

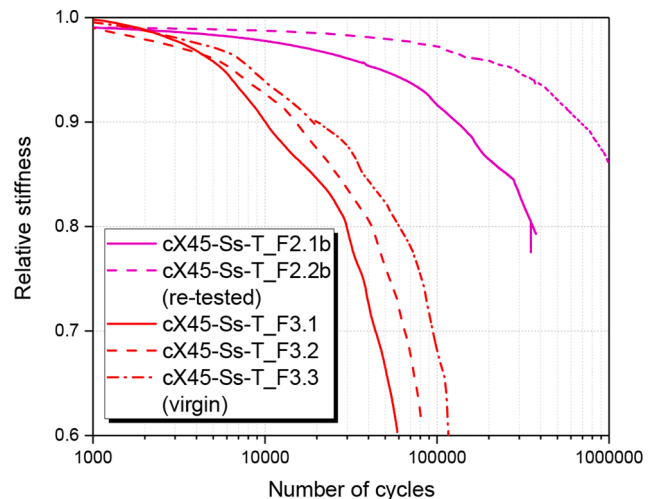


Fig. 7. Influence of re-testing on stiffness degradation of wrapped composite joints – cyclic tests at 212 MPa nominal stress range in the brace.

part as shown in Fig. 8 (c). This demonstrates that the wrapped composite joints can have fatigue endurance which is comparable to endurance of the non-welded details of steel circular hollow sections.

All the welded joints failed at the welded detail. The cracks initiated in the chord on crown toe location and progressed toward chord saddle as shown in Fig. 8 (d). The largest SCF according to DNV-RP-C203 (2016) [36] is in the location chord saddle. Once the global stiffness degradation of the welded joints of more than 50% was reached, and crack developed across more than 50% of the circumference, the cyclic loading was stopped.

The DIC results were recorded at min and max load for the load cycles at which significant accumulated increment of the joint stiffness degradation (more than 0.4%) was registered. For each specimen, approximately 200 of such min/max load measurement pairs were recorded. The debonding length is determined from DIC results by tracing the growth of the zone with the increased surface strain, i.e. comparing the increased strains zone at the  $n$ th cycle and the initial state at the first cycle. The strain increases zone on the composites surfaces can indicate both the composite-to-steel debonding failure as well as the smeared material damage and delamination within the composite wrap. The governing failure mode by debonding at the composite-to-steel interface was confirmed by post-test cutting of the specimens. To this purpose, major principal strains were extracted along the surface curves on the brace members indicated in Fig. 8 (a). Example of principal strains at max load in initial and  $n$ th cycle along the brace member is shown in Fig. 9. There is substantial level of noise in the DIC measurement because of relatively low level of strains (0.5%) that are measured. The influence of noise on crack propagation analysis was eliminated by mathematical smoothing (filtering) of the strain curves. The filtered initial and the  $n$ th strain and max load curves were compared and a threshold of the difference between the filtered curves was chosen to determine the cut-off point of the debonded part in each  $n$ th cycle. A threshold of 0.015% of filtered strain difference was found as appropriate in a sensitivity study to distinguish between the zones with and without the debonding crack. The resulting debonding lengths  $a$  at the top and bottom braces of different specimens are plotted in Fig. 10

against loading cycles. It shows that the debonding crack extended initially at a high rate up to 60 mm and 100 mm for the nominal stress range of 141 MPa and 212 MPa, respectively, but propagated with a much lower rate in the second stage. The crack propagation rate at the steady, second stage,  $da/dn$  is calculated by obtaining the tangent slope as shown in Fig. 10 (a). Separate (independent) crack propagation rates were calculated for the top and bottom braces of each specimen. Propagation rates for different specimens and braces are summarised in Table 4 and plotted against the nominal stress range in Fig. 11. A linear model was proposed as Eq. (4) for characterising the relationship between crack propagation rate and the nominal stress range in the brace:

$$\frac{da}{dn} = c_1 (\Delta\sigma_{nb})^{c_2} \quad (4)$$

where  $c_1$  and  $c_2$  are model parameters and are determined by curve fitting as  $1.05 \times 10^{-32}$  and 12.58, respectively. The simple model in Eq. (4) can be used for preliminary crack propagation analysis and prediction of fatigue life of a wrapped joint at 45° angle at various load levels.

#### 4.4. Preliminary S-N curve of wrapped composite joint

S-N curves for welded steel details in many design codes (DNV-RP-C203 (2016) [36], IIW Recommendations [37], Eurocode 3 [38], etc.) are defined for the number of cycles at the end of initiation life as it represents the more than 90% of the total life of a welded joint, also confirmed in our own experiments shown in Fig. 5 (a) and (b). Wrapped composite joint on contrary, show gradual development of stiffness degradation and fatigue life can be defined only by setting explicit threshold on stiffness degradation. The experiments executed in this research show that wrapped composite joints do not fail even with stiffness degradation of 40%. In order to define the preliminary S-N curve of the wrapped joints, different levels of allowable stiffness degradation (5% – 40%) are taken as criterions shown in Fig. 12. The least square method regressions were conducted based on test data points from 3 different stress levels to form the S-N curve for each allowable stiffness degradation level. Virgin tested specimens from both

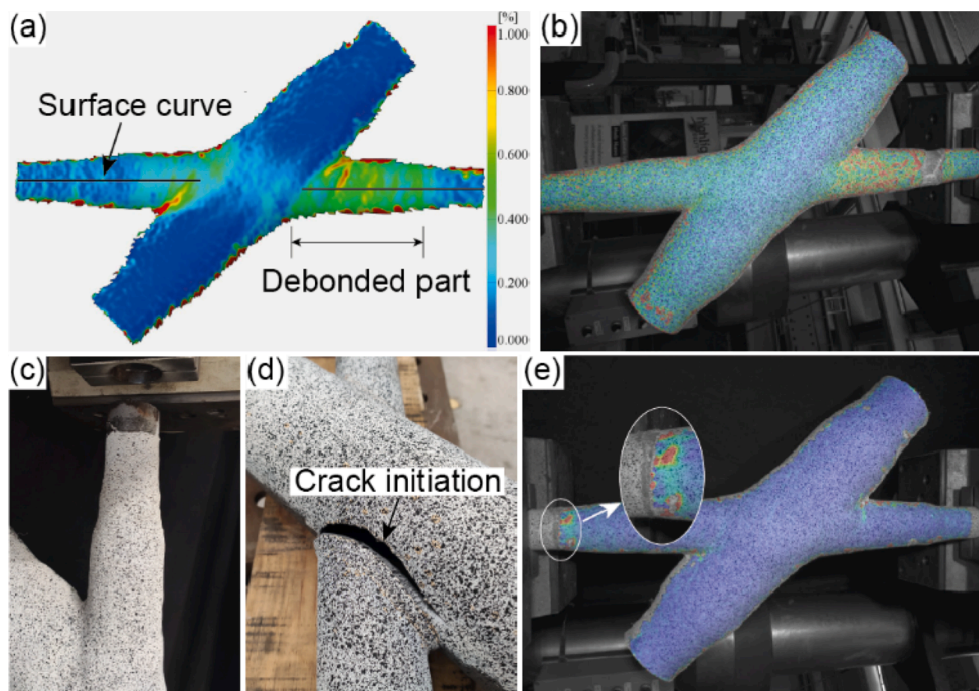


Fig. 8. Failure modes of wrapped composite and welded joints (a) typical debonding at the composite-to-steel interface (b) debonding/delamination of cX45-Ss-T\_F3.3 during fatigue loading (c) fracture of steel tube of cX45-Ss-T\_F2.1b during fatigue load (d) failure of welded joints (e) full debonding during static test after fatigue loading.

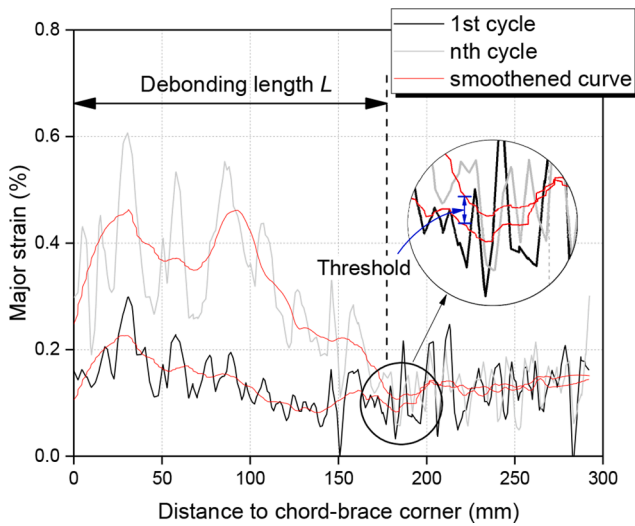


Fig. 9. Definition of debonding length (example for bottom brace of specimen cX45-Ss-T\_F3.1; cycle  $n = 42,426$ ).

the batches with the higher and lower roughness,  $R_z \approx 90 \mu\text{m}$  and  $R_z \approx 45 \mu\text{m}$ , respectively, were included in generation of the S-N curves. For each stress level, at least two results were considered for wrapped composite joints (from multiple specimens) and data points representing average number of cycles per stress range are shown. Number of cycles obtained for 5% stiffness degradation at all stress levels is actual. To assess potential S-N curves allowing larger degree of damage, the number of cycles at lower stress level (141 MPa and 85 MPa) are extrapolated based on regression of degradation curves shown in Fig. 5 (a) and (b) and the linear models presented in Fig. 6. The stress range indicated on the vertical axis is the nominal stress in the steel brace members, therefore comparable to nominal stresses in brace members of welded joints. S-N curves for welded tubular joints (class T in air) from DNV-RP-C203 (2016) [36] are also shown on the graph for the comparison reasons. In order to be able to compare the wrapped and welded joints on the basis of nominal stress in the brace the class T S-N curve from DNV is divided by Stress Concentration Factor  $SFC = 7.7$  which was the maximum value at the chord saddle location for the considered dimensions and angle of the welded joints. Data points obtained from 4 reference experiments on welded joint specimens are also shown in Fig. 12. The S-N curve B1 from DNV representing the characteristic fatigue endurance of non-welded circular hollow sections (S355), as well

as the S-N curve C1 representing characteristic fatigue endurance of CHS with circumferential butt weld made from both sides is also presented for comparison. The welded joint specimens were delivered with weld improvement by grinding, which provides improvement of fatigue life of joint by factor of 3.5 according to DNV-RP-C203 (2016) design recommendation. Satisfactory agreement between experiment results on weld

Table 4  
Crack propagation rates of different specimens.

Load ranges (kN)	Nominal stress ranges (MPa)	Specimen	Brace	Crack propagation rate (mm/cycle)	Average value (mm/cycle)
10–110	141	cX45-Ss-T_F2.1a	Top	0.000006	0.000016
		T_F2.1a	Bottom	0.000011	
		cX45-Ss-T_F2.2a	Top	0.000020	
		T_F2.2a	Bottom	0.000026	
15–165	212	cX45-Ss-T_F3.1	Top	0.0036	0.0022
		T_F3.1	Bottom	0.0012	
		cX45-Ss-T_F3.2	Top	0.0026	
		T_F3.2	Bottom	0.0012	
		cX45-Ss-T_F3.3	Top	0.0018	
		T_F3.3	Bottom	0.0027	

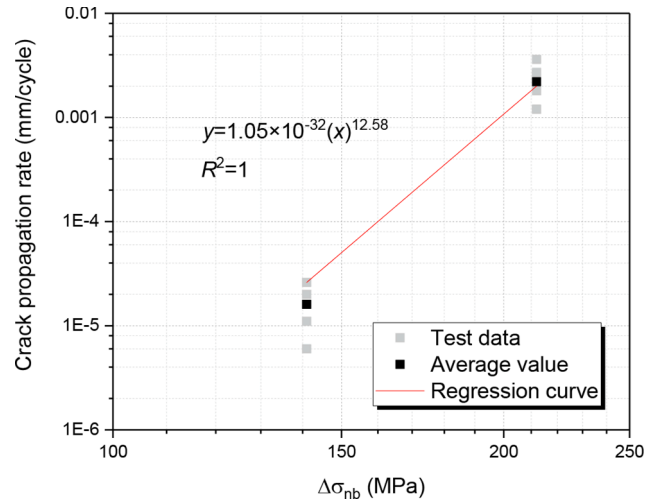
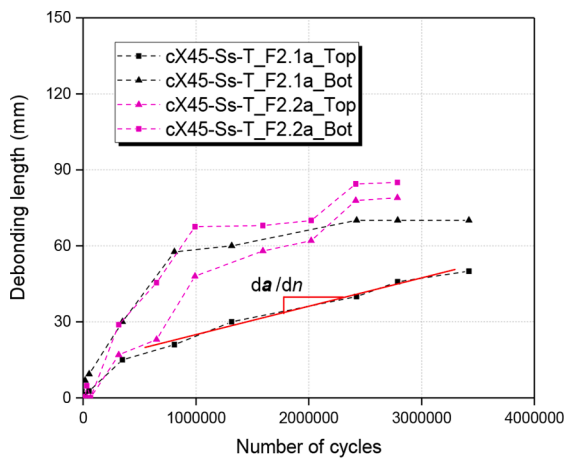
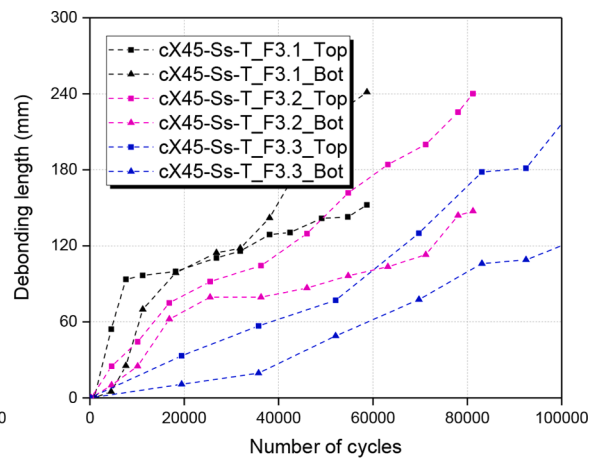


Fig. 11. Relationship between crack propagation rate and nominal stress range in the brace.



(a)



(b)

Fig. 10. Debonding crack propagation. (a) 10-110kN ( $\Delta\sigma_{nb} = 141\text{MPa}$ ) (b) 15-165kN ( $\Delta\sigma_{nb} = 212\text{MPa}$ ).

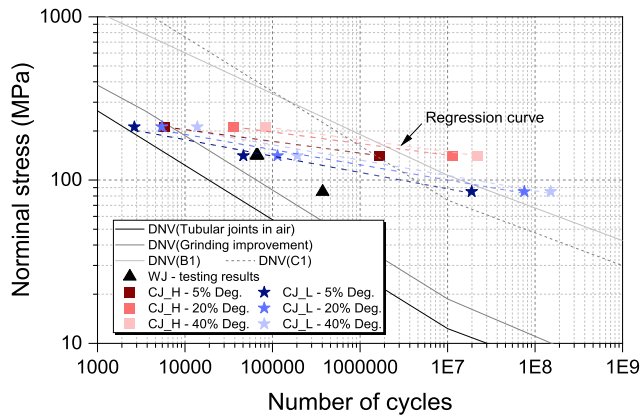


Fig. 12. Comparison of S-N curves of wrapped composite joints (CJ\_H with higher roughness, CJ\_L with lower roughness) and welded joints (WJ).

ed joints and S-N curve for grinded joint from DNV is found. The slope of the curve and the experiment data points is comparable. The relative difference in number of cycles of approx. 1 decade ( $\times 10^1$ ) from experiments and S-N curve from DNV is due to the fact that the S-N curve from DNV is based on characteristic values of multiple experiments.

The conclusion is that wrapped composite joints, even with the lower roughness, show superior fatigue performance vs. welded counterparts when the lowest damage tolerance for stiffness degradation of only 5% is allowed. Such superior performance is especially present in range of high number of cycles ( $n > 1e6$  and further) corresponding to the lower load range. Under higher load range, fatigue performance of composite joints with lower roughness show comparable or a little bit lower fatigue life than welded ones when the lowest damage tolerance is considered as a failure criterion. The fatigue life of wrapped composite joints is greatly improved in the low cycle (high load) range, as well in the high-cycle range, when enough roughness is guaranteed as clearly shown in Fig. 12. Generally speaking, the fatigue life of tested composite joints subjected to tension-tension cyclic loading is 10–100 times longer than their welded counterparts under the same stress range. The same conclusion can also be obtained by comparison of slopes of S-N curves. For S-N curves of wrapped composite joints, the negative inverse slope  $m$  is approximately 13.9 and 10.5 in case of higher and lower roughness, respectively, which is much higher than that of welded tubular joints ( $m = 3$  or 4 [36]). In terms of comparison with B1 and C1 curves, it can be concluded that wrapped composite joints are able to have longer fatigue life than the connected circumferentially welded or even non-welded steel members in high-cycle load range ( $n > 1e7$ ) which is dominant for fatigue design of offshore structures.

#### 4.5. Failure modes inspection on a micro-scale

In this section, a detailed analysis of failure mechanisms was carried out for wrapped composite joints on a micro-scale. A typical specimen cX45-Ss-T\_F3.3, which failed during fatigue loading by full debonding, was chosen to be inspected. This specimen was cut through its mid-plane after testing as shown in Fig. 13. The cut surfaces were grinded by sand paper and polished. It can be seen from the figure that the top brace has slid away from the chord and was fully debonded along the brace-to-composite interface. Debonding by peeling also occurred at a small portion of the chord-to-composite interface near the sharp corner. Except for debonding, there are delamination marks present between different composite layers and fracture of composites as well, which occurs near the end of the wrapped part.

For the bottom brace, macro-scale failure mechanisms are not obvious. Observation is continued on micro-scale with magnification of  $50\times$  and  $250\times$ . For both braces, inspection locations include sharp corner of the composite wrapping and several points along the brace-to-

composite interface as shown in Fig. 13 with the aim to check failure mechanism development. Four distinct locations A, B, C and D are analysed in Fig. 14 (a) and (b) for the top (full debond) and the bottom brace (partial debond), respectively. Detail A shows crack on the wrapping surface in the sharp corners for both top and bottom braces, which was also observed in DIC results (see stress concentration in Fig. 8 (a)). These cracks however only extend to a limited depth through a resin rich layer at the wrapping surface and do not seem to jeopardize the integrity of the composite plies in the corner. For the top brace, which definitely fully debonded, point B shows a typical debonding mechanism where there is a layer of crashed matrix debris between the composite laminate and steel surface. Debonding on the top brace developed until the point C where fracture of composite laminate occurred. Point D on the opposite side of the top brace shows location where debonding of the composite-to-steel interface switches to delamination inside the composite laminate and fracture of the first plies. This means that the failure mechanism may be different around the circumference of the brace. The bottom brace suffered much less debonding. An obvious gap between the composite laminate and the steel surface of the brace tube could only be identified at point B in Fig. 13 (b). Point C, further away from the joint root, shows no visible signs of debonding. Limited debonding and resin debris are observed up to and in the point D.

#### 4.6. Influence of surface roughness of steel tubes

The surface roughness of steel adherent [28–31] is known to be an important factor which influences the mechanical behaviour of a bonded joint. It is shown in in Fig. 5 (c) and Table 3 that specimens produced in a batch with apparently lower surface roughness exhibited much higher rate of stiffness degradation.

The average maximum profile height  $R_z$  was used to quantify the surface roughness of steel tubes from the two batches as it is regularly related to performance of bonded interfaces. According to literature, the shear strength of bonded joints will increase as  $R_z$  increases from 10 to  $140\ \mu\text{m}$  [39], although some references [40] reported that there is a plateau at  $R_z = 45\ \mu\text{m}$  after which the bonding strength may even exhibit a decrease with the increasing roughness. In general, the conclusions from the previous research related to monotonic behaviour can be different for the cyclic behaviour investigated here. Definition of  $R_z$  is

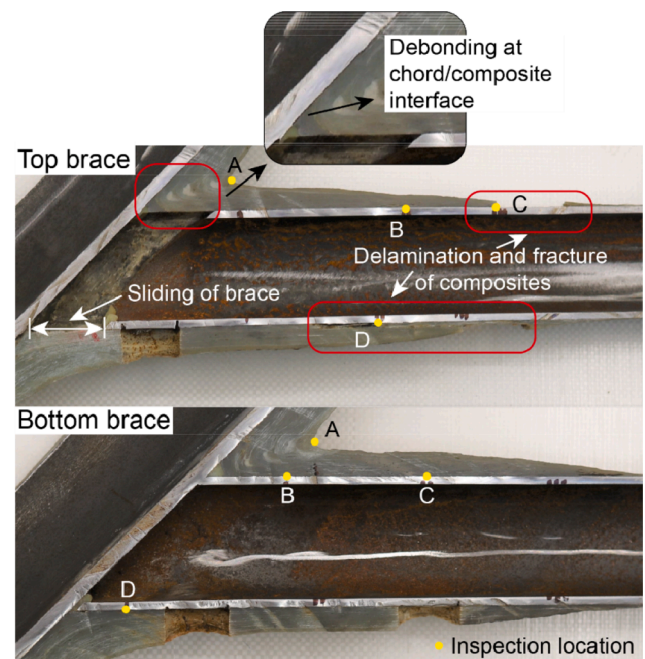


Fig. 13. Inspection of cut surface.

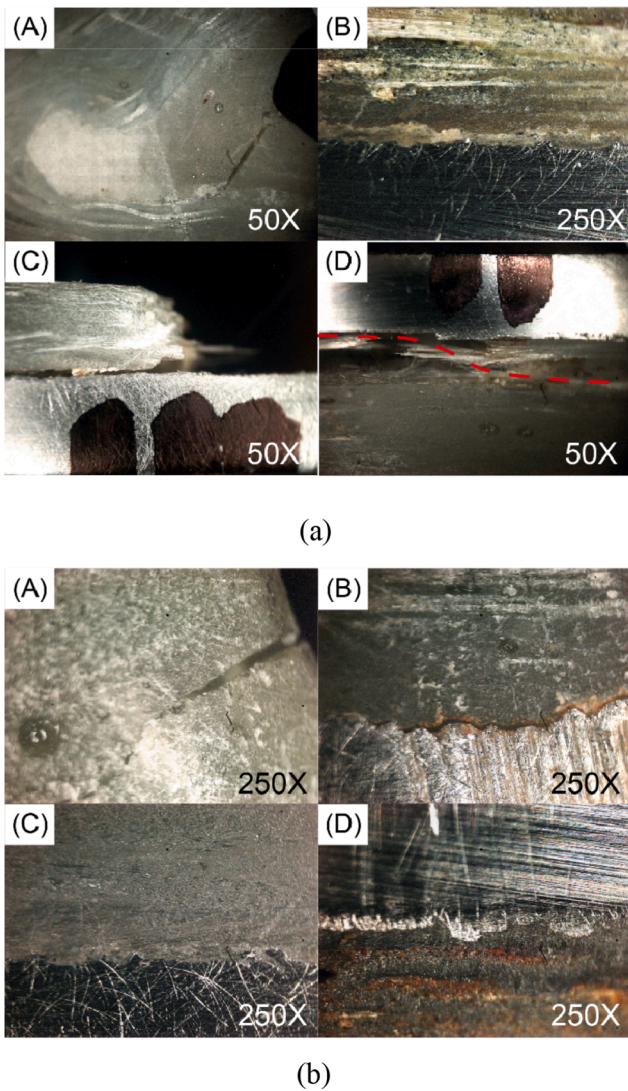


Fig. 14. Microscale inspection of composite-to-steel interface. (a) top brace (b) bottom brace.

shown in Eq. (5) and Fig. 15. It describes the average maximum profile height of the roughness features within five times the sampling length  $l_r$  ( $5l_r$  equals the total evaluation length  $l_n$ ):

$$R_z = \frac{1}{5} \sum_{i=1}^5 R_{zi} \quad (5)$$

points on each brace of specimens cX45-Ss-T\_F3/4 were measured with Marsurf PS 10 profilometer. The measurement was done before application of the composite material.

The measuring results are summarized in Table 5. Between the two series of specimens, it was shown that average values of  $R_z$  for cX45-Ss-T\_F3 (series 3) ranges from 90 to 100  $\mu\text{m}$ , approximately 1.2 to 2 times of those for cX45-Ss-T\_F4 (series 4), which ranges from 44 to 85  $\mu\text{m}$ . Correspondingly, the stiffness degradation rate of specimens cX45-Ss-T\_F4 in the secondary study stage is about 6 times larger than that of specimens cX45-Ss-T\_F3 according to Table 3. Relationship between the stiffness degradation rate and the surface roughness is given in Fig. 16. The horizontal axis in Fig. 16 represents the minimum average  $R_z$  within the top or bottom brace of the specimen (underline averages in Table 5) which is dominant for the stiffness degradation process. As it can be expected, a higher surface roughness of steel tubes leads to a lower stiffness degradation rate. Very correlated dependency of stiffness degradation rate vs.

surface roughness is found. More detailed research in future could propose linear or asymptotic interpolation models to predict the stiffness degradation rate by a known (measured) surface roughness, as illustrated in Fig. 16.

The mechanism of the beneficial effect of increased surface roughness on fatigue performance can be further explained by Fig. 17, which shows representative profiles with different  $R_z$ . It can be seen that profiles with higher  $R_z$  exhibits deeper valleys, resulting in larger contact areas between adherends, such that the mechanical interlocking and surface energies are increased [27,41]. The results indicate that uniform and controlled surface roughness is crucial for consistent fatigue performance of the bonded interface and control of scattering of the behaviour.

#### 4.7. Residual static resistance of wrapped composite joints

After stiffness degradation up to 40% in cyclic load test at two higher load ranges (series F2 and F3), monotonic static load was applied to determine the residual static resistance of the specimens. All the specimens failed due to full de-bonding of the composite-to-steel interface in the follow-up monotonic load test. Force-displacement behaviour of specimens with previous cyclic loading is compared in Fig. 18 (a) to those of reference specimens cX45-Ss-T\_S1.1/2 [42] which did not experience any cyclic (fatigue) loading. All of the specimens showed decreased initial stiffness in the follow-up monotonic load test which corresponds to stiffness reduction due to partial damage (debonding) during cyclic load. The specimen with lowest stiffness degradation (approx. 20%) after more than 3 mil. cycles of load, cX45-Ss-T\_SF2.2b, shows no reduction of static resistance. The other two specimens with significant (>40%) stiffness degradation during the cyclic load test show up to 30% reduction of static resistance.

Table 6 shows dependency of stiffness degradation in each specimen and the residual static resistance. It should be noted that the global stiffness degradation used to control and decide on stopping the cyclic loading is the average value of degradation of top and bottom brace-to-chord joints. However, one side is always suffering more damage, see Fig. 10, which means that one side degraded more while the other side degraded less than the target stiffness degradation limit of 40%. Therefore, the separate stiffness degradation of the top or bottom brace is calculated with help of DIC results and presented in Table 6. The value of maximum stiffness degradation of top or bottom is correlated to the relative residual static resistance in Fig. 18 (b).

Although the values of specimens with very high stiffness degradation (>50%) show an obvious decrease of static resistance, the results presented indicate that wrapped composite joints have the potential to sustain its original axial tension resistance even after experiencing substantial stiffness degradation of 20% due to cyclic (fatigue) load.

## 5. Conclusions

Fatigue behaviour of wrapped composite joints of Circular Hollow Sections was evaluated by cyclic axial tension load experiments in this

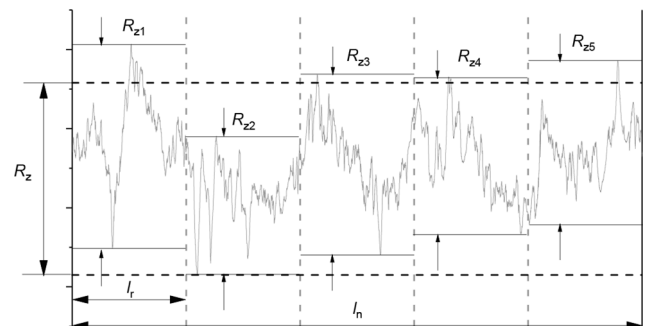
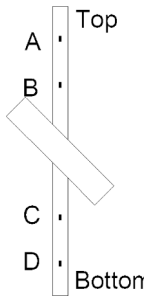


Fig. 15. Definition of  $R_z$ .

**Table 5**  
Summary of  $R_z$  of different specimens ( $\mu\text{m}$ ).

Position		Specimens						
		cX45-Ss-T_F3.1	cX45-Ss-T_F3.2	cX45-Ss-T_F3.3	cX45-Ss-T_F4.1	cX45-Ss-T_F4.2	cX45-Ss-T_F4.3	
	Top	A	100	85	97	42	45	46
		B	99	103	94	87	57	48
		Top average	99.50	94	95.50	64.50	51	47
		C	91	83	106	137	67	42
		D	88	89	105	73	60	40
		Bottom average	89.50	86	105.50	105	63.50	41
Minimum average			89.5	86	95.5	64.5	51	41

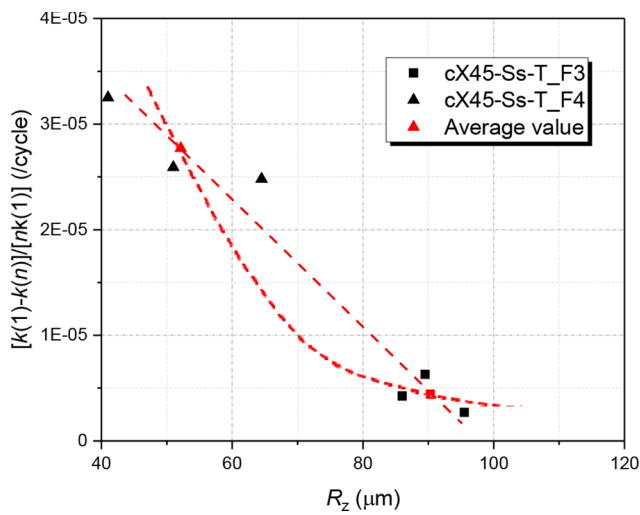


Fig. 16. Effect of roughness on stiffness degradation rate.

paper. Small-scale wrapped composite and welded specimens of CHS X-joints with 45° angle between  $\phi 60.3 \times 4 \text{ mm}$  brace and  $\phi 108 \times 5 \text{ mm}$  chord member were loaded by tension–tension axial load on braces in constant amplitude cyclic regime. Fatigue performance of wrapped composite joints is compared to that of reference specimens of welded joints and preliminary S-N curves are presented. Initiation and propagation of stiffness degradation is analysed through strain distribution and failure modes inspected with help of 3D DIC system and micro camera. The

influence of load range, re-testing and surface roughness of steel tubes on fatigue behaviour of wrapped composite joint was studied. After fatigue tests, monotonic loads were applied to the joints to investigate the influence of cyclic loads on the residual static resistance. From studies mentioned above, main conclusions can be drawn as follows:

- Preliminary S-N curves are obtained for the debonding failure mode of wrapped composite joints considering different levels of damage tolerance (5–40%) and surface roughness. Even with the lowest considered damage tolerance where allowable stiffness degradation is considered to be only 5%, wrapped composite joints with lower roughness still show superior fatigue performance vs. welded ones. Fatigue life of tested composite joints subjected to tension–tension cyclic loading is 10–100 times longer than that of their welded counterparts under the same stress range. The negative inverse slope  $m$  of the wrapped composite joint S-N curve is approximately 13.9 and 10.5 in case of higher and lower roughness, respectively, which is much higher than that of welded tubular joints ( $m = 3$  or 4).
- The wrapped composite joints exhibited superior fatigue performance than their welded counterparts both in terms of number of cycles to failure and damage tolerance. Welded specimens failed abruptly after crack initiation at only up to 5% stiffness degradation, while stiffness of wrapped composite joints degraded steadily up to 40%. Only 2 out of 14 specimens exhibited failure in cyclic load tests with up to 3 mil cycles. Specimens loaded under lowest load range, corresponding to 85 MPa nominal stress range in the brace tubes, show almost no stiffness degradation up to 3 million cycles which leads to estimate of practically infinite fatigue life.
- Stiffness degradation of wrapped composite joints was mainly due to debonding of the composite-to-steel interface. Specimens were

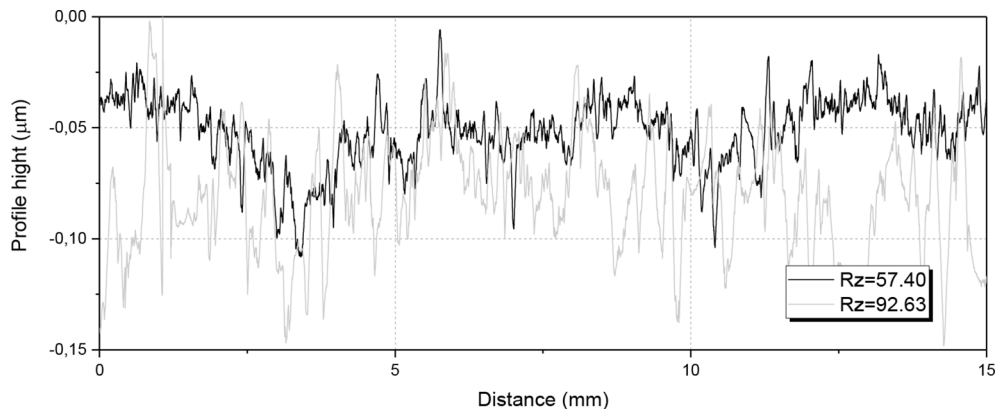
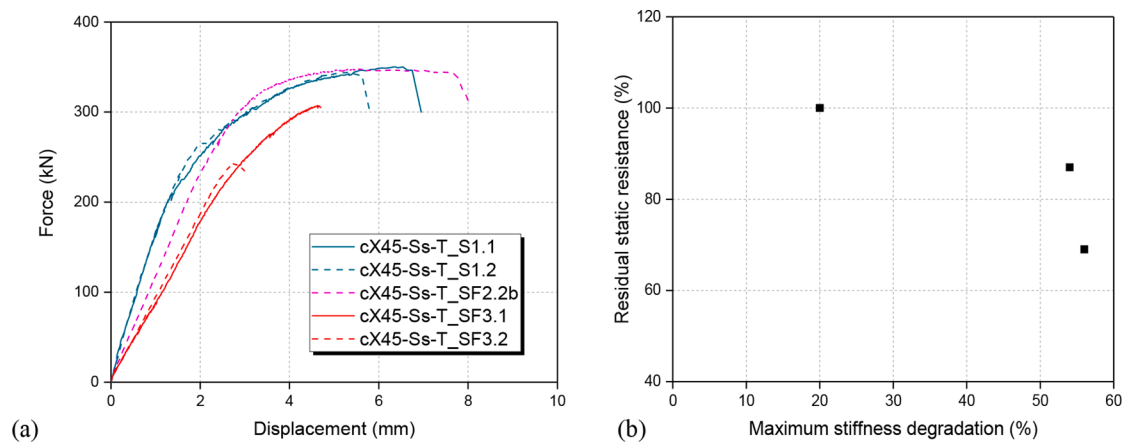


Fig. 17. Representative roughness profiles with high and low  $R_z$ .



**Fig. 18.** Static behaviour of wrapped composite joints after cyclic load tests. a) Load-displacement vs. original static tests form [42]. (b) Residual static resistance vs. maximum stiffness degradation.

**Table 6**

Residual static resistance in function of stiffness degradation in cyclic load tests.

Specimen	Initial stiffness – whole specimen (kN/mm)	Stiffness after cyclic load test – whole specimen (kN/mm)	Stiffness reduction – whole specimen (%)	Stiffness reduction – bottom DIC (%)	Stiffness reduction – top DIC (%)	Static resistance (kN)	Residual static resistance after cyclic test* (%)
cX45-Ss-T_S1.1	137	–	–	–	–	354	–
cX45-Ss-T_S1.2	136	–	–	–	–	349	–
cX45-Ss-T_SF2.2b	130	100	23%	13%	20%	352	100
cX45-Ss-T_SF3.1	139	84	40%	54%	37%	307	87
cX45-Ss-T_SF3.2	138	84	39%	33%	56%	244	69

\*Static resistance of specimens after cyclic loading compared to the average static resistance of reference specimens.

designed with sufficient thickness of the composite wrap to promote and study the debonding as critical failure mode. In a structure the composite wrap would be designed to fail first once the fatigue behaviour of the interface is well known. Except for debonding, one of the wrapped composite joints even fractured at the steel tube outside of the wrapped part, which demonstrates that the wrapped joints can have fatigue endurance which is comparable and exceeding that of the non-welded details of steel circular hollow sections.

- During the re-testing scheme, specimens tested by a low and then by a high load range exhibited approximately 10 times lower stiffness degradation rate than the virgin specimens that were only tested at high load range.
- Influence of surface roughness of steel obtained by grit blasting is significant. Increase of average maximum roughness  $R_z$  from 45  $\mu\text{m}$  to 90  $\mu\text{m}$  led to 5 to 6 times decrease of stiffness degradation rate, i.e. 5–6 times extension of the fatigue life.
- Residual static resistance after more than 3 million load cycles leading to 20% stiffness degradation remains without any reduction and the joint can still sustain the load equivalent to yield resistance of the steel brace CHS. Static resistance of the wrapped composite joints that suffered 56% stiffness reduction by cyclic (fatigue) load is reduced by 30%.

This paper demonstrates that non-welded wrapped composite joints have huge potential to provide outstanding fatigue performance of joints in fatigue dominated CHS structures. Wrapped composite joints open possibility to greatly improve current lifetime performance and economic feasibility limitations of CHS structures made with welded joints.

## CRediT authorship contribution statement

**Weikang Feng:** Investigation, Data curation, Writing – original draft, Visualization. **Marko Pavlovic:** Conceptualization, Methodology, Supervision, Writing – review & editing, Project administration, Fund-acquisition.

## Declaration of Competing Interest

The authors declare that they have no known competing financial interests or personal relationships that could have appeared to influence the work reported in this paper.

## Acknowledgement

The authors are grateful to Dutch Research Council (NWO) for financially supporting the experiments presented in this paper through “Fatigue resistant Wrapped FRP Joints of Structural Hollow Sections” NWO Demonstrator 2018 project, grant No. 16949. The first author also would like to express his gratitude for the financial support from China Scholarship Council (CSC) under grant number of 201906260300.

## References

- [1] Wardenier J, Packer J, Zhao X, van der Vegte G. *Hollow sections in structural applications*. 2nd ed. Geneva: CIDECT; 2010.
- [2] Haldimann-Sturm SC, Nussbaumer A. Fatigue design of cast steel nodes in tubular bridge structures. *Int J Fatigue* 2008;30:528–37. <https://doi.org/10.1016/j.ijfatigue.2007.03.007>.
- [3] Zhao XL, Zhang L. State-of-the-art review on FRP strengthened steel structures. *Eng Struct* 2007;29:1808–23. <https://doi.org/10.1016/j.engstruct.2006.10.006>.

- [4] Jiao H, Zhao XL. CFRP strengthened butt-welded very high strength (VHS) circular steel tubes. *Thin-Walled Struct* 2004;42:963–78. <https://doi.org/10.1016/j.tws.2004.03.003>.
- [5] Haedir J, Bambach MR, Zhao XL, Grzebieta RH. Strength of circular hollow sections (CHS) tubular beams externally reinforced by carbon FRP sheets in pure bending. *Thin-Walled Struct* 2009;47:1136–47. <https://doi.org/10.1016/j.tws.2008.10.017>.
- [6] Lesani M, Bahaari MR, Shokrieh MM. Numerical investigation of FRP-strengthened tubular T-joints under axial compressive loads. *Compos Struct* 2013;100:71–8. <https://doi.org/10.1016/j.compstruct.2012.12.020>.
- [7] Lesani M, Bahaari MR, Shokrieh MM. Experimental investigation of FRP-strengthened tubular T-joints under axial compressive loads. *Constr Build Mater* 2014;53:243–52. <https://doi.org/10.1016/j.conbuildmat.2013.11.097>.
- [8] Lesani M, Bahaari MR, Shokrieh MM. FRP wrapping for the rehabilitation of Circular Hollow Section (CHS) tubular steel connections. *Thin-Walled Struct* 2015;90:216–34. <https://doi.org/10.1016/j.tws.2014.12.013>.
- [9] Fu Y, Tong L, He L, Zhao XL. Experimental and numerical investigation on behavior of CFRP-strengthened circular hollow section gap K-joints. *Thin-Walled Struct* 2016;102:80–97. <https://doi.org/10.1016/j.tws.2016.01.020>.
- [10] Fam A, Witt S, Rizkalla S. Repair of damaged aluminum truss joints of highway overhead sign structures using FRP. *Constr Build Mater* 2006;20:948–56. <https://doi.org/10.1016/j.conbuildmat.2005.06.014>.
- [11] Pavlovic M, Veljkovic M, Bogers P. Method for making a virgin joint between two separate structural hollow sections, and such a virgin joint. IPC No. E04C, E04B.
- [12] Pavlovic M, Veljkovic M, Liatzouras M. Wrapped FRP joints of steel hollow sections. In: Proceedings of the 8<sup>th</sup> International Conference on Thin-walled Structures. Lisbon, Portugal, July 24-27, 2018.
- [13] He P, Pavlovic M. Feasibility of wrapped FRP circular hollow section joints In: Proceedings of the 17<sup>th</sup> International Symposium on Tubular Structures. Singapore, December 9-12, 2019. Doi: 10.3850/978-981-11-0745-0 043-cd.
- [14] Rathnakar G, Shivanand HK. Effect of thickness on flexural properties of epoxy based glass fiber reinforced laminate. 2012; 2: 409–12.
- [15] Fatchurrohman N, Sulaiman S, Sapuan SM, Ariffin MKA, Baharuddin BHTT. Analysis of a metal matrix composites automotive component. *Int J Automot Mech Eng n.d.*;ISSN:2531–40. Doi: 10.15282/ijame.11.2015.32.0213.
- [16] Zakaria KA, Jimit RH, Ramli SNR, Aziz AA, Bapokutty O, Ali MB. Study on fatigue life and fracture behaviour of fibreglass reinforced composites. *J Mech Eng Sci* 2016;10:2300–10. <https://doi.org/10.15282/jmes.10.3.2016.8.0214>.
- [17] Al-Alkawi HJ, Al-Fattal DS, Ali A-JH. Types of the fiber glass-mat on fatigue characteristic of composite materials at constant fiber volume fraction: experimental determination. *Al-Khwarizmi Eng J* 2012; 8.
- [18] Mini KM, Lakshmanan M, Mathew L, Mukundan M. Effect of fibre volume fraction on fatigue behaviour of glass fibre reinforced composite. *Fatigue Fract Eng Mater Struct* 2012;35:1160–6. <https://doi.org/10.1111/j.1460-2695.2012.01709.x>.
- [19] Abd Allah MH, Abdin EM, Selmy AI, Khashaba UA. Effect of fibre volume fraction on the fatigue behaviour of GRP pultruded rod composites. *Compos Sci Technol* 1996;56:23–9. [https://doi.org/10.1016/0266-3538\(95\)00125-5](https://doi.org/10.1016/0266-3538(95)00125-5).
- [20] Quaresimin M, Talreja R. Fatigue of fiber reinforced composites under multiaxial loading. *Fatigue Life Predict. Compos Compos Struct, Elsevier Inc.* 2010:334–89. <https://doi.org/10.1533/9781845699796.2.334>.
- [21] Vassilopoulos AP, Keller T. *Fatigue of Fiber-reinforced Composites*. London: Springer London; 2011. Doi: 10.1007/978-1-84996-181-3.
- [22] Brøndsted P, Lilholt H, Lystrup A. Composite materials for wind power turbine blades. *Annu Rev Mater Res* 2005;35:505–38. <https://doi.org/10.1146/annurev.matsci.35.100303.110641>.
- [23] Zhao X-L, Al-Mahaidi R, Liu HB. The effect of fatigue loading on bond strength of CFRP bonded steel plate joints. In: Proceedings of the International Symposium on Bond Behaviour of FRP in Structures. Hong Kong, December 7-9, 2005.
- [24] Doroudi Y, Fernando D, Zhou H, Nguyen VT, Ghafoori E. Fatigue behavior of FRP-to-steel bonded interface: An experimental study with a damage plasticity model. *Int J Fatigue* 2020;139:105785. <https://doi.org/10.1016/j.ijfatigue.2020.105785>.
- [25] Zhang Y, Vassilopoulos AP, Keller T. Stiffness degradation and fatigue life prediction of adhesively-bonded joints for fiber-reinforced polymer composites. *Int J Fatigue* 2008;30:1813–20. <https://doi.org/10.1016/j.ijfatigue.2008.02.007>.
- [26] Zhang L, Cao S, Tao X. Experimental Study on Interfacial Bond Behavior between CFRP Sheets and Steel Plates under Fatigue Loading. *Materials (Basel)* 2019;12:377. <https://doi.org/10.3390/ma12030377>.
- [27] Azari S, Papini M, Spelt JK. Effect of surface roughness on the performance of adhesive joints under static and cyclic loading. *J Adhes* 2010;86:742–64. <https://doi.org/10.1080/00218464.2010.482430>.
- [28] Prolongo SG, Rosario G, Ureña A. Study of the effect of substrate roughness on adhesive joints by SEM image analysis. *J Adhes Sci Technol* 2006;20:457–70. <https://doi.org/10.1163/156856106777144345>.
- [29] Şekerçioğlu T, Rende H, Gülsöz A, Meran C. The effects of surface roughness on the strength of adhesively bonded cylindrical components. *J Mater Process Technol* 2003;142:82–6. [https://doi.org/10.1016/S0924-0136\(03\)00463-1](https://doi.org/10.1016/S0924-0136(03)00463-1).
- [30] Shahid M, Hashim SA. Effect of surface roughness on the strength of cleavage joints. *Int J Adhes Adhes* 2002;22:235–44. [https://doi.org/10.1016/S0143-7496\(01\)00059-8](https://doi.org/10.1016/S0143-7496(01)00059-8).
- [31] de Barros S, Kenedi PP, Ferreira SM, Budhe S, Bernardino AJ, Souza LFG. Influence of mechanical surface treatment on fatigue life of bonded joints. *J Adhes* 2017;93:599–612. <https://doi.org/10.1080/00218464.2015.1122531>.
- [32] John W. Bull. Numerical Analysis and Modelling of Composite Materials. Netherlands: Springer; 1996. Doi: 10.1007/978-94-011-0603-0.
- [33] International Standard Organization. ISO 14126:1999, Fibre-reinforced plastic composites — Determination of compressive properties in the in-plane direction. <https://www.iso.org/standard/23638.html> (accessed April 6, 2021).
- [34] International Standard Organization. ISO 527-1:2019, Plastics — Determination of tensile properties — Part 1: General principles. <https://www.iso.org/standard/75824.html> (accessed April 6, 2021).
- [35] International Standard Organization. ISO 14129:1997, Fibre-reinforced plastic composites — Determination of the in-plane shear stress/shear strain response, including the in-plane shear modulus and strength, by the plus or minus 45 degree tension test method. <https://www.iso.org/standard/23641.html> (accessed April 6, 2021).
- [36] DNV GL. DNVGL-RP-C203: Fatigue design of offshore steel structures The. DNV GL - Recomm Pract 2016:176.
- [37] Hobbacher AF. IIW Collection Recommendations for Fatigue Design of Welded Joints and Components. Netherlands: Springer; 2016.
- [38] Arya C. Eurocode 3: Design of steel structures. *Des Struct Elem* 2015;3:395–453. <https://doi.org/10.1201/b18121-19>.
- [39] Saborowski E, Dittes A, Steinert P, Lindner T, Scharf I, Schubert A, et al. Effect of metal surface topography on the interlaminar shear and tensile strength of aluminum/polyamide 6 polymer-metal-hybrids. *Materials (Basel)* 2019; 12. Doi: 10.3390/ma12182963.
- [40] Hwang JH, Jin CK, Lee MS, Choi SW, Kang CG. Effect of surface roughness on the bonding strength and spring-back of a CFRP/CR980 hybrid composite. *Metals (Basel)* 2018;8:1–12. <https://doi.org/10.3390/met8090716>.
- [41] Packham DE. Surface energy, surface topography and adhesion. *Int J Adhes Adhes* 2003;23:437–48. [https://doi.org/10.1016/S0143-7496\(03\)00068-X](https://doi.org/10.1016/S0143-7496(03)00068-X).
- [42] He P, Pavlovic M. Static behavior of Wrapped Composite Joints for Circular Hollow Sections. Submitted to. *Eng Struct* 2020.